JOURNAL OF APPLIED PHYSICS 115, 183512 (2014)

Electron-beam induced variation of surface profile in amorphous $As_{20}Se_{80}$ films

Yu. Kaganovskii,[1,a)] M. L. Trunov,[2,a)] C. Cserhati,[3] P. M. Lytvyn,[4] D. L. Beke,[3] and S. Kökényesi[5]
[1]*Department of Physics, Bar-Ilan University, Ramat-Gan 52900, Israel*
[2]*Uzhgorod National University, Narodna sq. 3, Uzhgorod 88000, Ukraine*
[3]*Department of Solid State Physics, University of Debrecen, Bem sqr. 18/b, H-4026 Debrecen, Hungary*
[4]*Institute of Semiconductor Physics, NAS of Ukraine, Kiev 03028, Ukraine*
[5]*Department of Experimental Physics, University of Debrecen, Bem sqr. 18/b, H-4026 Debrecen, Hungary*

(Received 9 April 2014; accepted 29 April 2014; published online 14 May 2014)

Unusual profile variation of holographic surface relief gratings is detected in thin (2 μm) $As_{20}Se_{80}$ chalcogenide films under e-beam irradiation: gratings of small periods were smoothed, whereas the gratings of larger periods increased their amplitudes. Irradiation was carried out in SEM, with 20 kV voltage and 8 nA current; the profiles of the irradiated areas were analyzed both by AFM and SEM. It is found that the kinetics of both flattening and growth followed by exponential law and took place due to lateral mass transport accelerated by e-irradiation. It is shown that the profile variation is mainly caused by competition between capillary forces and "chemical" forces induced by broken and deformed atomic bonds under e-beam irradiation. The kinetics of profile variation was calculated assuming that the mechanism of e-beam induced mass transfer is volume diffusion. The diffusion coefficients were estimated from the experimental data using theoretical expressions derived. © *2014 AIP Publishing LLC*. [http://dx.doi.org/10.1063/1.4875838]

I. INTRODUCTION

Chalcogenide glasses (ChGs) containing S, Se, and Te, covalently bonded with elements of IV and V groups, such as As, Sb, Bi, Ge, etc., due to their wide optical transparency in the infrared (IR), have been recognized as materials of choice for applications in micro-optics, integrated optics, and IR spectroscopy.[1–3] ChGs exhibit a number of remarkable structural and optical changes when exposed to light or electron beams, such as photo-amorphization and photo-crystallization, changes in refractive index, photoexpansion and photodarkening, light induced fluidity, and dicroism.[4–7]

Among these phenomena, there is an increasing interest to photo-induced mass transport,[8–15] which is caused by capabilities to use this phenomenon for dry patterning of the films by laser or electron beams and thus to fabricate various optical elements (optical micro-lenses, gratings, waveguides) by a one-step technique. Multiple studies of interaction of electron beam with different ChGs[16–22] were carried out to find capabilities of dry fabrication of channel waveguides for micro-optics and integrated optics. In these studies, an electron beam scanned along a line in ChG films was changing their refractive index and surface profile.

Tanaka detected surface deformations,[16] such as convex relief lines with micrometer scales, in bulk and thin films of As_2S_3 under a line-scanned electron beam. The height and the width of the surface relief were found monotonically increasing with exposure time, accelerating voltage, and absorbing current. It was assumed that the deformation was produced by electrostatic force and electro-induced fluidity.

An expansion of the film surface under e-beam irradiation was also detected in amorphous Ge-S and Ge-Se films.[17] It was explained, using the model developed by Shimakawa *et al.*,[18,19] that the assumed repulsion between the layers is due to capture of injected electrons.

Later, in experiments with e-beam irradiated $Ge_{20}Se_{80}$ films,[20] it was found that mounds produced by low area doses transformed by large doses to trenches with slightly raised edges. The mound formation was explained as e-beam induced expansion, the trench formation at higher doses was attributed to excess charging of the film that pushed material to the sides of the beam. As seen, explanations of the phenomenon in different papers differed from one another, and no consistent description was presented.

Recently, we have demonstrated that electron irradiation, besides volume expansion, induced lateral mass transport in ChG films.[21] We carried out our experiments with $As_{20}Se_{80}$ films, which were found to be the most effective in patterning both by band gap light[22,23] and by electron beam.[24] Under a line-scanned electron beam, we have detected formation of mounds and depressions near the mounds that bear witness to lateral mass transport. We have calculated the kinetics of electron-induced variations of surface profile assuming that the main driving force of the lateral mass transport is a steady state electrostatic field, which appears due to lateral distribution of carriers generated by e-beam. As the main mechanism of the mass transport, we considered diffusion accelerated due to formation of radiation defects under irradiation. As a direct confirmation of e-beam induced mass transport, we have demonstrated flattening of periodic (3.6 μm) surface profiles, caused by capillary forces and accelerated due to irradiation by electrons.[21]

[a)]Authors to whom correspondence should be addressed. Electronic addresses: kagany@mail.biu.ac.il and trunov.m@gmail.com

0021-8979/2014/115(18)/183512/8/$30.00

In the present work, we describe unusual behavior of surface relief gratings (SRGs) preliminarily written in $As_{20}Se_{80}$ films, under electron irradiation: gratings of small periods are smoothed, whereas gratings of larger periods increase their amplitudes. Such variation of the grating profile cannot be explained in frames of previous conceptions. We propose an explanation of the phenomenon considering all possible driving forces causing e-beam induced lateral mass transport in the films. Besides, assuming diffusion mechanism of the mass transport, we calculate the kinetics of SRG flattening or enhancement.

II. EXPERIMENTAL

$As_{20}Se_{80}$ films of 2 μm thick were prepared by thermal vacuum (10^{-6} Torr) deposition on microscope glass slides covered by conductive layer of indium tin oxide (ITO). The gratings with the periods $\Lambda = 1.7$, 3.3, 7.5, and 10.5 μm were recorded on the film surface by two crossed p-polarized beams of a diode laser ($\lambda = 650$ nm). Initial amplitudes of the gratings varied from 80 to 150 nm. Then, the gratings and films without gratings (of the same area, for comparison) were irradiated by e-beam in SEM (Hithachi S-4300 CFE) using accelerating voltage $U = 20$ kV and electron current about 8 nA. Conductive ITO sub-layer prevented charging of the film during irradiation. In this regime, the continuously moving e-beam scanned (line-by-line) two different areas: $16 \times 8\ \mu m^2$ and $40 \times 20\ \mu m^2$, with the repetition rate 91.5 ms per rectangle, independently of the rectangle area. The beam direction was parallel to the grating vector. During 91.5 ms, the beam irradiated 40 lines, independently of the rectangle width, i.e., the linear beam speed was 17.5 μm/ms and 7 μm/ms for larger and smaller rectangles, respectively. Total irradiation time ranged from 10 s to 240 s for both rectangles. This corresponded to average area doses varied from $0.85 \times 10^4\ \mu C/cm^2$ to $1.3 \times 10^6\ \mu C/cm^2$ in different experiments. After illumination, the surface profiles were scanned by atomic force microscope (AFM).

III. RESULTS

The main result consists in the following: gratings with periods $\Lambda = 1.7\ \mu$m and 3.3 μm were smoothed under e-beam irradiation, whereas the grating with periods 7.5 μm and 10.5 μm were enhanced. Fig. 1 shows, as an example, typical AFM images of gratings with $\Lambda = 1.7\ \mu$m and 7.5 μm after e-beam irradiation for various times. One can see two successive stages of flattening of 1.7 μm gratings and enhancement of 7.5 μm grating (grating amplitude is increased inside the irradiated square). Analysis of appropriate grating profiles (Fig. 2) shows that the grating amplitudes, h, vary with time following exponential law (Fig. 3), i.e.,

$$h(t) = h_0 \exp(-\kappa \cdot t)\ , \tag{1}$$

where h_0 is the initial amplitude and κ is the flattening/enhancement constant, which is positive for gratings of small periods and negative for gratings with large periods.

IV. DISCUSSION

The main idea used for the explanation of SRG flattening/enhancement is based on lateral e-beam induced mass transport caused by several competitive driving forces: capillary forces (determined by the Laplace pressure), which are caused by the curvature of the surface profile, electrical forces, which appear during e-beam irradiation, and chemical forces caused by deformation and breakage of atomic bonds under e-irradiation. Mass transport is induced in all radial directions around the beam; we are interested, however, in a profile evolution in the x-direction, parallel to the grating vector. Thus, we have to analyze how the mass transport and the local profile evolution (around the beam) depend on the film thickness, which varies due to SRG in the x-direction as

$$H(x,t) = H_0 + h(t) \sin qx. \tag{2}$$

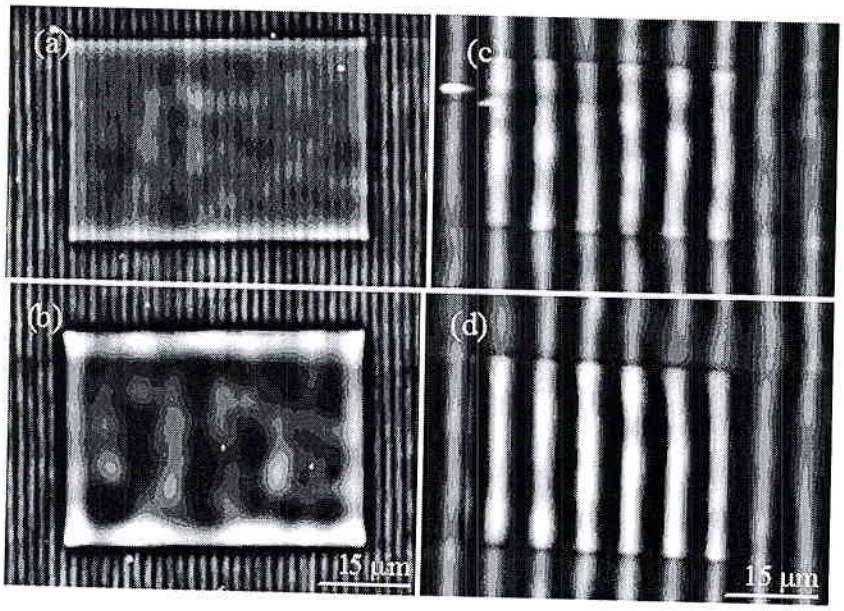

FIG. 1. Typical AFM images of successive stages of flattening of 1.7 μm surface relief gratings [(a) and (b)] and enhancement of 7.5 μm grating [(c) and (d)] under e-beam irradiation of rectangular area $20 \times 40\ \mu m^2$. $U = 20$ kV, $I_e = 8$ nA. (a)—$t = 60$ s and (b)—120 s; (c)—120 s and (d)—240 s.

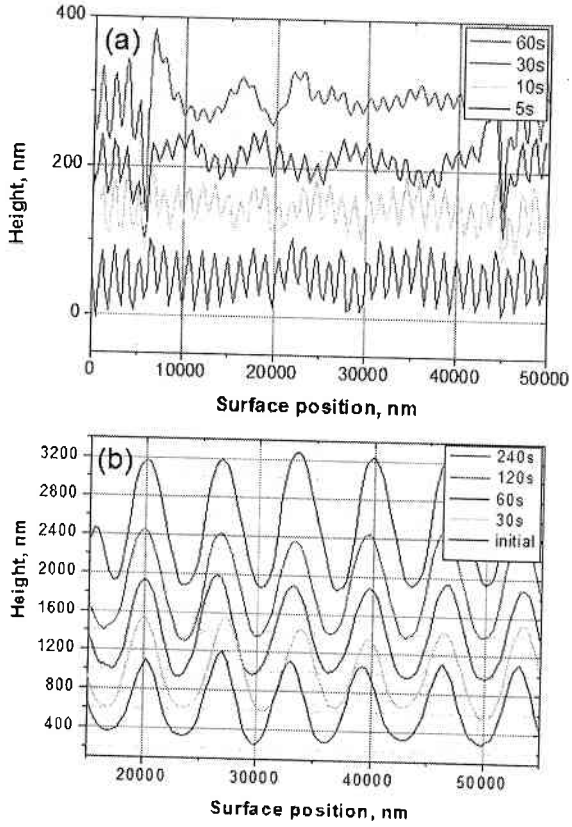

FIG. 2. Surface profiles at successive stages of flattening for 1.7 μm grating (a) and enhancement of 7.5 μm grating (b).

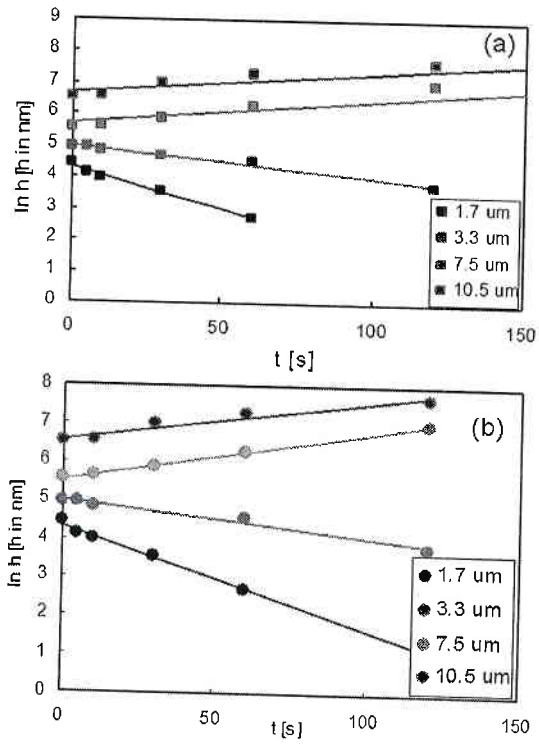

FIG. 3. Flattening kinetics of SRG with the periods $\Lambda = 1.7$ and 3.3 μm and enhancement for $\Lambda = 7.5$ and 10.5 μm. (a)—Irradiated area $16 \times 8\,\mu m^2$; (b)—irradiated area $40 \times 20\,\mu m^2$.

Here, $h(t)$ is the grating amplitude, which varies with the time of irradiation, t, $q = 2\pi/\Lambda$ is the grating wave number, and Λ is the grating period. We show below that capillary forces aspire to flatten the surface profile and cause mass transfer directed from thicker to thinner surface areas. Electrical forces, which induce mass transport around the e-beam, do not depend on the film thickness. The chemical forces induce mass transfer directed in our case from thinner to thicker areas of the film, as it will be discussed later. As a result, flattening or enhancement of the SRG depends on competition between capillary and chemical forces. We have found that "chemical" force is independent of the grating wavenumber, q, whereas capillary force is proportional to q^3. As a result, depending on the grating period, enhancement or flattening of SRG occurs.

A. Carrier generation and radiation defects

In our experiments, an e-beam of 100 nm in diameter continuously scans along parallel lines in the x-direction (parallel to the grating vector) with the rate of 17.5 μm/ms for larger irradiated rectangles and 7 μm/ms for smaller rectangles.

We made simulation of the beam power distribution in the depth of $As_{20}Se_{80}$ film using CASINO program.[25] We have found that for the average film thickness $H_0 = 2\,\mu$m and accelerating voltage 20 keV used in our experiments, the power losses, $-dP/dz = G(z)$, versus penetration depth, z, can be estimated as a shifted Gaussian[26,27]

$$G(z) = G_m \exp[-(z - z_0)^2/Z^2]$$

with $z_0 = 160$ nm and $Z = 800$ nm (Fig. 4). The depth z_0 corresponds to the maximum losses. Some shift of the maximum losses from the surface to z_0 is caused by particular feature of inelastic electron scattering in the material: single scattering near the surface transforms to the multiple scattering with the depth z. The losses are proportional both to the electron energy, which drops with z, and to the number of scattered electrons, which grows with z.

In the radial directions, the interaction volume can be modeled as a cylinder of height H and radius R ($R \approx H_0/2$). With these parameters, the power absorbed by the film

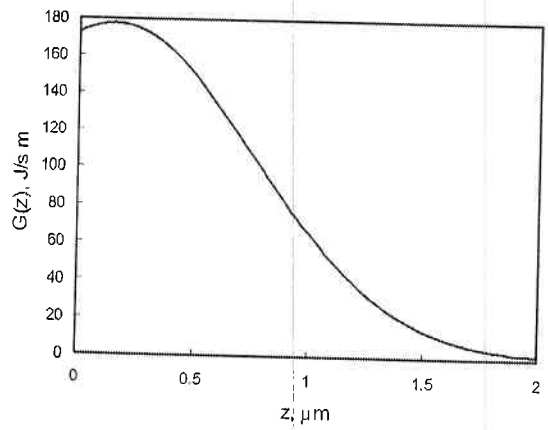

FIG. 4. Depth distribution of power losses calculated by CASINO program for 2-μm $As_{20}Se_{80}$ film irradiated by 20 kV e-beam.

$$P = \int_0^H G(z)dz = \frac{G_m Z\sqrt{\pi}}{2}\left(erf\frac{z_0}{Z} + erf\frac{H - z_0}{Z}\right),$$

depends on the film thickness H: the thicker the film the higher power is absorbed. Direct estimates show, however, that variation of P with the film thickness for our experimental conditions are less than 0.2%, so that one can neglect this variation.

The energy losses are caused mainly by generation of electron–hole pairs within the interaction volume. The average generation rate per unit volume of the irradiated part, g, depends on the film thickness and can be calculated[28] as

$$g(x,t) \approx g_0\left[1 - \frac{h(t)}{H_0}\sin qx\right], \quad g_0 = \frac{P}{\chi E_g \pi R^2 H_0}, \tag{3}$$

where E_g is the band gap of the film material, and χ represents an efficiency factor that includes losses due to backscattering, ionization, and phonon interactions. As $h/H_0 \ll 1$, we have replaced $1/(1 + h/H_0)$ for $1 - h/H_0$.

The generated free carriers move from the irradiated volume to all lateral directions and change the local electrical properties of the material. As the electrons and holes have different mobilities, their radial distribution results in formation of an internal steady state electric field, $E(\rho)$, which accelerates slower carriers and slows down faster carriers (ρ is measured from the center of the beam and $\rho = 0$ is the axis of the beam). In the $As_{20}Se_{80}$ films, mobility of holes exceeds mobility of electrons and, thus, the steady state electric field should be directed towards the irradiated volume. Taking into account, the formation of the electric field, one can write the hole and electron currents as

$$j_p = -D_p\frac{dp}{d\rho} + p\frac{D_p}{kT}eE; \quad j_n = -D_n\frac{dn}{d\rho} - n\frac{D_n}{kT}eE. \tag{4}$$

Here, e is the electron charge, $n(\rho)$, $p(\rho)$ and D_n and D_p are the local *dimensionless* concentrations and the diffusion coefficients of electrons and holes, respectively, and $E(\rho)$ is the lateral electric field. The steady state carrier distribution corresponds to equality of electron and hole currents ($j_n = j_p$); to satisfy the neutrality condition, one can suppose $n - n_0 = p - p_0$ (n_0 and p_0 are the electron and hole concentrations without irradiation) and, thus, $dp/d\rho = dn/d\rho$. Then, the steady state electric field is

$$E = \frac{kT}{e}\frac{D_p - D_n}{pD_p + nD_n}\frac{dn}{d\rho} \tag{5}$$

and

$$j_p = j_n = -D_{amb}\frac{dp}{d\rho}; \quad D_{amb} = \frac{(n+p)D_nD_p}{nD_n + pD_p}. \tag{6}$$

Here, D_{amb} is the ambipolar diffusion coefficient.[29]

The radial steady state distribution of dimensionless electron concentration, $n(\rho)$, can be found from the following differential equation:[28]

$$D_{amb}\nabla^2 n(\rho) + g\Omega - \frac{n(\rho)}{\tau} = 0. \tag{7}$$

Here, g is the generation density and n/τ is the recombination density, τ is the electron lifetime before recombination with holes, and Ω is the average atomic volume of the film material. Writing $\nabla^2 n(\rho)$ in cylindrical coordinates and introducing the carrier diffusion length, $l = \sqrt{D_{amb}\tau}$, which is the same for electrons and holes, one can rewrite Eq. (7) in the form

$$\frac{1}{\rho}\frac{dn}{d\rho} + \frac{d^2n}{d\rho^2} - \frac{n}{l^2} = \begin{cases} -\frac{g\Omega\tau}{l^2} & 0 < \rho \le R \\ 0 & \rho > R \end{cases}. \tag{8}$$

We suggest that the carrier generation occurs inside the interaction volume ($0 < \rho < R$). Differential Eq. (8) was solved under following boundary conditions. The first condition was that there should be no additional (non-equilibrium) carriers at infinite distance from the generation volume. Further, the electron density function and its first derivative were supposed to be continuous. We obtain

$$n(\rho,x) = n_0 + \begin{cases} \frac{[1 - K_1(R/l)\cdot I_0(\rho/l)]P\Omega\tau}{\chi E_g \pi R^2 H_0 \alpha}\left(1 - \frac{h}{H_0}\sin qx\right) & 0 < \rho \le R \\ \frac{I_1(R/l)\cdot K_0(\rho/l)P\Omega\tau}{\chi E_g \pi R^2 H_0 \alpha}\left(1 - \frac{h}{H_0}\sin qx\right) & \rho > R \end{cases}. \tag{9}$$

Here, n_0 is initial electron concentration (before irradiation), I_0, I_1, K_0, and K_1 are the Bessel functions, $\alpha = K_1(R/l)I_0(R/l) + K_0(R/l)I_1(R/l)$. The concentration of holes can be calculated from Eq. (8) using electro neutrality condition: $p(\rho) = p_0 + n(\rho) - n_0$ (p_0 is the initial hole concentration). As seen, the concentration of carriers generated by e-beam is proportional to the beam power, P, lifetime τ, and depends on the film thickness. Typical radial distribution $n(\rho)$ calculated using Eq. (9) for our experimental conditions and $x = 0$ is shown in Fig. 5.

Amorphous $As_{20}Se_{80}$ is known as a photoconductive p-type semiconductor. After generation and redistribution, electrons and holes are localized around P and C atoms (P denotes pnictide atom and C—chalcogen) forming relatively stable configurations—valence alternation pairs (VAP), called also as self-trapped excitons (STE), which can be

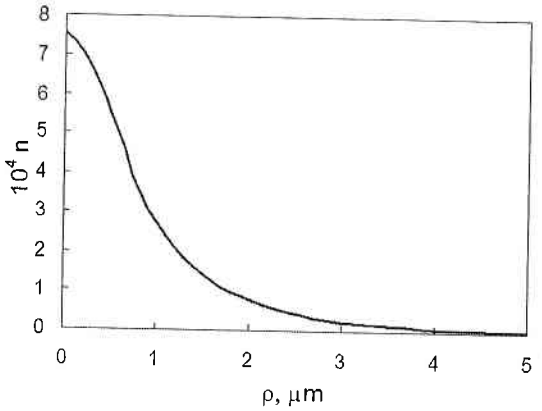

FIG. 5. Radial dimensionless concentration distribution of electrons generated inside and near the irradiated volume. $P = 160\,\mu$W, $\chi = 1.5$, $H_0 = 2\,\mu$m, $R = 1\,\mu$m.

considered as radiation defects.[6] The STE concentration, n_{ex}, is proportional to the concentration of generated electrons and holes, i.e., one can write $n_{ex} = \xi\, n$. Due to deformation and breakage of bonds, these defects can accelerate atomic jumps compared to their thermal diffusion without irradiation.[30] As a result, diffusion coefficients of both chalcogens and pnictides become higher inside and near the interaction volume, i.e., e-beam induces mass transport in irradiated areas of the film. As it follows from Eq. (9), the concentration of radiation defects periodically vary with the x-coordinate and maxima of $n_{ex}(x)$ correspond to minima of $H(x)$. Maximal effect of irradiation should be observed near the irradiated volume ($\rho \le R$), where n is the highest.

B. Kinetics of the mass transport

As we mentioned above, irradiation by a focused electron beam induces mass transport in all radial directions around the beam; the profile evolution, however, occurs due to dependence of the mass redistribution on the x-coordinate, parallel to the grating vector. Thus, we have to analyze how the mass transport and the local profile evolution (around the beam) depend on the film thickness, H. Previously, analyzing the kinetics of patterning and capillary flattening of SRGs under illumination by a polarized bandgap light[13,15,31] and by electron irradiation,[21,24] we found that the main mechanism of the mass transport is volume diffusion accelerated under irradiation due to creation of radiation defects. The mass transport kinetics is determined by the effective diffusion coefficient, $D = D^P c + D^C(1-c)$ (D^P and D^C are diffusion coefficients of P and C atoms, respectively, and c is the concentration of P atoms in the film material). The diffusion coefficients are proportional to the concentration of the radiation defects, n_{ex}.

Taking into account all possible driving forces of the mass transport, we present chemical potential of atoms as the following sum:

$$\mu = \mu_0 + \mu_{Ch} + \mu_L + \mu_E. \tag{10}$$

Here, μ_0 is the bulk chemical potential of the atoms without irradiation; for simplicity, we do not distinguish between P and C atoms. The second term, μ_{Ch}, is a "chemical" contribution in μ caused by irradiation: $\mu_{Ch}(\rho,x) = \varepsilon \cdot n_{ex}(\rho,x)$, where ε is the increase of the energy caused by deformation and breaking of chemical bonds around the radiation defect. The energy ε includes also stresses caused by the irradiation-induced volume expansion of the film. The third term, μ_L, takes into account contribution of capillary forces (Laplace pressure) caused by the curvature of the surface profile $\zeta(x) = h \sin qx$. Chemical potential μ_L depends both on x and z coordinates (z axis is directed from the surface into the bulk of the film) and its distribution inside the film satisfies the Laplace equation

$$\nabla^2 \mu_L = 0 \tag{11}$$

and boundary conditions

$$\mu_L(x,0) = K\Omega\gamma; \quad \mu_L(x,H_0) = 0. \tag{12}$$

Here, $K(x) \approx -\zeta''_{xx}$ is the local surface curvature (for small surface slopes), γ is the surface tension, and Ω is the average atomic volume. Solution of Eq. (11) with the boundary conditions (12) yields

$$\mu_L(x,z) = \frac{e^{q(H_0-z)} - e^{-q(H_0-z)}}{e^{-qH_0} - e^{qH_0}}\,\gamma\,\Omega q^2 h \sin qx. \tag{13}$$

The last term in Eq. (10), μ_E, represents contribution of electrostatic forces caused by formation of steady state electric field, $E(\rho)$, around e-beam. As it follows from Eqs. (5) to (9), with $n \gg n_0$ and $p \gg p_0$, i.e., with $n \approx p$ (in the interaction volume), $E(\rho)$ does not depend on the film thickness H. Thus, considering contribution of different driving forces in e-beam induced flattening/enhancement gratings, one can neglect electrostatic force.

The chemical driving force can be given as

$$\begin{aligned} f_{Ch} &= -\frac{\partial \mu_{Ch}}{\partial \rho} = -\varepsilon \frac{\partial n_{ex}(\rho,x)}{\partial \rho} \\ &= -\varepsilon \frac{P\Omega\xi\tau K_1(R/l)\, I_1(\rho/l)}{l\alpha\chi E_g \pi R^2 H_0}\left(1 - \frac{h}{H_0}\sin qx\right). \end{aligned}$$

The diffusion flux caused by the chemical force is

$$\begin{aligned} J_{Ch}(\rho,x) &= \frac{D}{kT\Omega} f_{Ch} \\ &= -\varepsilon \frac{DP\xi\tau K_1(R/l)\, I_1(\rho/l)}{l\alpha\chi E_g \pi R^2 H_0 kT}\left(1 - \frac{h}{H_0}\sin qx\right). \end{aligned} \tag{14}$$

Mass redistribution induced by J_{Ch} around the beam in the interaction volume depends on the film thickness (varies with the x-coordinate). Variation of the surface profile caused by the chemical force near the beam axis ($\rho = 0$) is

$$\left(\frac{d\zeta}{dt}\right)_{Ch} = -\Omega H\, \nabla J_{Ch} = -H\frac{\Omega}{\rho}\frac{\partial}{\partial \rho}(J_{Ch}\rho). \tag{15}$$

As the diffusion coefficient, D, can be presented in the form $D = D^0 n_{ex} = D^0 \xi\, n$, after substitution of Eqs. (9) and (14) into Eq. (15), we obtain near the beam axis ($\rho \approx 0$)

$$\left(\frac{d\zeta}{dt}\right)_{Ch} = \frac{D^0\xi^2}{kT}\frac{P^2\Omega^2\tau^2 K_1(R/l)[\alpha - K_1(R/l)]}{\pi^2 R^4 H_0^2 \chi^2 E_g l^2 \alpha}\varepsilon \cdot \zeta.$$

Capillary (Laplace) force, $-\nabla\mu_L$, depends both on x and z coordinates [see Eq. (13)] and induces flattening of the gratings. The kinetics of the profile evolution under Laplace pressure is determined by the diffusion fluxes normal to the surface at $z \approx 0$

$$\left(\frac{d\zeta}{dt}\right)_L = -J_z(x,0)\Omega = -\frac{D}{kT}\frac{\partial\mu_L(x,z)}{\partial z}\bigg|_{z=0} = -\frac{D\Omega\gamma}{kT}\frac{e^{qH_0}+e^{-qH_0}}{e^{qH_0}-e^{-qH_0}}q^3\zeta.$$

Taking into account both chemical and capillary forces, we have

$$\frac{\partial\zeta}{\partial t} = \left(\frac{\partial\zeta}{\partial t}\right)_{Ch} + \left(\frac{\partial\zeta}{\partial t}\right)_L = (A\varepsilon + Bq^3)\zeta. \quad (16)$$

Here,

$$A = \frac{D^0\xi^2}{kT}\frac{P^2\Omega^2\tau^2 K_1(R/l)[\alpha - K_1(R/l)]}{\pi^2 R^4 H_0^2 \chi^2 E_g l^2 \alpha};$$
$$B = \frac{D\Omega\gamma}{kT}\frac{e^{qH_0}+e^{-qH_0}}{e^{qH_0}-e^{-qH_0}}.$$

Solving Eq. (16) with the initial condition $h(0) = h_0$, we obtain

$$h(t) = h_0\exp(-\kappa t); \quad \kappa = -(A\varepsilon + Bq^3). \quad (17)$$

The flattening constant, κ, consists of two terms, which have opposite signs. The first term describes the diffusion flux under effective pressure caused by radiation defects; the flux is directed from thinner parts of the film (with negative curvature), where the density of radiation defects is higher, towards thicker parts (with positive curvature), where the density of defects is lower. The second term describes competitive opposite flux from positive to negative curvatures of the profile caused by capillarity. The first term in Eq. (17) does not depend on q, whereas the second term is proportional to q^3.

Due to competition between capillary forces and chemical driving forces induced by irradiation, constant κ (q) changes its sign at some wave number $q^* = (-A\varepsilon/B)^{1/3}$: κ is negative with $q < q^*$ and positive with $q > q^*$. Dependence $\kappa(q)$ calculated with the use of Eqs. (16) and (17) is presented in Fig. 7 as a solid line. The parameters used for calculations are given in Table I.

The calculations show that $q^* = 1.65\,\mu m^{-1}$ corresponds to the grating period $\Lambda^* = 2\pi/q^* \approx 3.8\,\mu m$. This explains flattening of gratings with periods $\Lambda = 1.7$ and $3.3\,\mu m$ and enhancement of gratings with $\Lambda = 7.5$ and $10\,\mu m$.

C. Comparison with the experiment

As it was mentioned above, under our irradiation conditions, the e-beam moved along lines subsequently (line-by-line) irradiating rectangular area. It is clear that real time of irradiation, t_{irr}, i.e., time, during which the e-beam interacts with the ChG film, is much shorter than the exposure time t and can be estimated as

$$t_{irr} = t\frac{R}{Lk_l}. \quad (18)$$

Here, L is the width of the irradiated rectangular area and k_l is the number of lines, which e-beam passes irradiating the rectangle (in our experiments, $k_l = 40$). Indeed, the e-beam interacts with the each spot in the rectangle during time $\Delta t \approx R/v$ (v is the speed of the moving e-beam). E-beam returns to the same spot after passing distance Lk_l (for time Lk_l/v). With this speed, e-beam is shifted for a distance of the order of $R \approx 1\,\mu m$ during 0.057 ms for larger rectangle and 0.14 ms for smaller rectangle. This time can be given as time of e-beam interaction with the film during one area

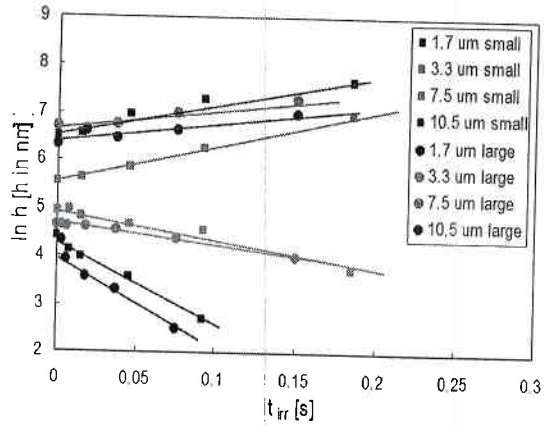

FIG. 6. Plots $ln\ h$ vs real irradiation time, t_{irr}, for various grating periods Λ and two irradiated rectangles.

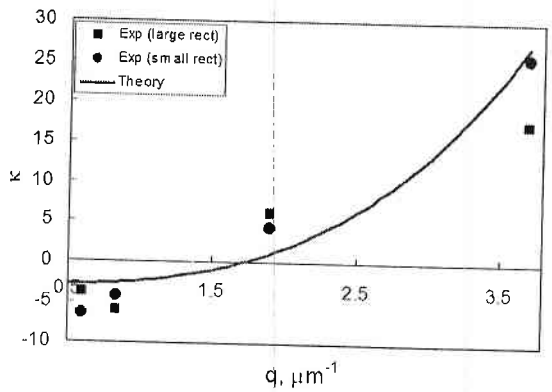

FIG. 7. Comparison of experimental data on flattening/enhancement SRGs (squares and circles) with the calculated dependence κ (q). The theoretical curve corresponds to $D = 2.1 \times 10^{-10}$ m^2/s and $\varepsilon = 0.44$ eV.

TABLE I. Parameters used for calculations.

P, μW	Ω, cm^3	τ, μs (Ref. 32)	R, μm	χ	E_g, eV	H_0, μm	l, μm	h_0, nm
160	2×10^{-23}	2	1	2	2	2	1	150

scan. As follows from Eq. (18) that $t = 100$ s exposure time corresponds to $t_{irr} = 62.5$ ms real irradiation time for larger rectangles ($L = 40\,\mu$m) and 156 ms for smaller rectangles ($L = 16\,\mu$m). In Fig. 6, we show our results on flattening/enhancement of SRGs (Fig. 3) as the function of the real irradiation time, t_{irr}. The slopes of the lines give the flattening/enhancement constants, κ, for various grating periods, Λ. As seen, the slopes for smaller and larger irradiated areas are close to each other. The constants κ calculated for various SRG wave numbers from the slopes of the straight lines in Fig. 6 are presented in Fig. 7 (as squares and circles) in comparison with the calculated dependence $\kappa\,(q)$. To get agreement between the theory and experiments, we used two fitting parameters: the diffusion coefficient $D = D^0 n_{ex}$ and the energy ε associated with radiation defects. Variation of ε shifts the calculated dependence $\kappa\,(q)$ up or down in Fig. 7 and results in a variation of q^* too. The change of D (or D^0) stretches or compresses the $\kappa\,(q)$ function in vertical direction. Using Maple program for the best fitting of calculated dependence $\kappa\,(q)$ to experimental data, we have found that $D = 2.1 \times 10^{-10}\,\mathrm{m^2/s}$ and $\varepsilon = 0.44$ eV. Inasmuch, we assumed $D = D^0 n_{ex} = D^0 \xi\, n$, with $n \approx 7.3 \times 10^{-4}$ (inside the interaction volume, see Fig. 5) and $\xi \approx 0.4$, we obtain $D^0 \approx 7 \times 10^{-7}\,\mathrm{m^2/s}$.

Recently, we studied patterning and SRG flattening on a surface of $As_{20}Se_{80}$ films under e-beam irradiation.[21,24] The electron energy and other experimental conditions were similar to those in the current studies. From the kinetics of ridge formation, as well from the flattening kinetics, we determined e-beam accelerated diffusion coefficient and reported $D \approx 1.4 \times 10^{-13}\,\mathrm{m^2/s}$, i.e., about 3 orders of magnitude smaller compared to that reported here. This difference happened because, in our previous papers, the beam power was about 10% smaller compared to current study and the irradiation time was taken, by mistake, as exposure time. As it can be seen from Eq. (18), exposure time t and irradiation time t_{irr} differ by a factor of 10^3.

It is worth to compare diffusion coefficients accelerated by e-beam (D) and by band gap light (D_l). In our previous studies of SRG flattening under illumination by band gap polarized light,[27] the photo-induced diffusion coefficient was found to be proportional to the light intensity: $D_l = \beta I$ with $\beta = 2.5 \times 10^{-18}\,\mathrm{m^4/J}$.

Number of generated electron-hole pairs, N, under illumination by band gap light may be found from the equation

$$\frac{dN}{dt} = \frac{\alpha_l \cdot I}{E_g} - \frac{N}{\tau} = 0. \tag{19}$$

Here, α_l is the light absorption coefficient and I is the light intensity. The term $\alpha_l \cdot I/E_g$ gives a number of photons absorbed in unit volume per unit time, i.e., approximately a number of electron-hole pairs generated in unit volume per unit time. After some short time $t \ll \tau$, these pairs are transformed in STE, and $n_{ex} = \xi\, n \approx \xi\, N\, \Omega$. As it follows from Eq. (19)

$$n_{ex} = \alpha_l I\, \Omega\, \xi\, \tau / E_g. \tag{20}$$

Presenting D_l as $D_l^0 n_{ex}$ and using Eq. (20), we obtain

$$\beta = D_l^0 \alpha_l \Omega \xi \tau / E_g. \tag{21}$$

Substitution in Eq. (21) $\Omega \approx 2 \times 10^{-29}\,\mathrm{m^3}$, $E_g \approx 2$ eV, $\alpha_l \approx 5 \times 10^5\,\mathrm{m^{-1}}$, $\xi \approx 0.1$, and $\beta = 2.5 \times 10^{-18}\,\mathrm{m^4/J}$ gives $D_l^0 = 4 \times 10^{-7}\,\mathrm{m^2/s}$. This value is in a rather good agreement with $D^0 \approx 7 \times 10^{-7}\,\mathrm{m^2/s}$ obtained in experiments with e-beam induced mass transport. Thus, both band gap light and electron irradiation accelerate diffusion by similar way, due to generation of radiation defects.

As it follows from the atomic diffusion theory,[33] the accelerated diffusion coefficient can be estimated as

$$D \approx \frac{1}{2} a^2 \nu_0 n_{ex} \exp(-Q_m/kT). \tag{22}$$

Here, a is the length of diffusion jump, ν_0 is the frequency of atomic oscillations, Q_m is the migration energy, and n_{ex} is the concentration of radiation defects (free volumes), which define a probability to meet the free volume near migrating atom.

As seen from Eq. (22)

$$D^0 \approx \frac{1}{2} a^2 \nu_0 \exp(-Q_m/kT). \tag{23}$$

Putting typical values $a^2 \approx 10^{-19}\,\mathrm{m^2}$, $\nu_0 \approx 10^{13}\,\mathrm{s^{-1}}$, and $D^0 \approx 7 \times 10^{-7}\,\mathrm{m^2/s}$ in Eq. (23), we find that the migration energy of atoms into a free volume is very low, less than 0.1 eV. This small photo-induced migration energy is possible, if we assume that diffusing atoms are charged and Coulomb interaction between electrons and holes associated with P and C atoms near STE should also be taken into account.

Considering the problem of irradiation induced mass transport, it is important to note that the local heating effect of e-beam irradiation can be neglected. Previously, it was shown[21,34] that the increase of the film temperature can be estimated as

$$\delta T = \frac{kP}{2\pi \kappa_q R_e}. \tag{24}$$

Here, $k \approx 0.7$ is the fraction of the beam power, which is converted into heat, κ_q is the heat conductivity of the film, and R_e is the electron range. With $R_e \approx 2\,\mu$m, $\kappa_q \approx 1.2\,\mathrm{W/m \cdot K}$, and $P = 160\,\mu$W, we have $\delta T \approx 7$ K that cannot noticeably change the contribution of thermally activated diffusion compared to that accelerated by e-beam.

V. CONCLUSIONS

We have detected that SRGs written on a surface of $As_{20}Se_{80}$ ChG films can be smoothed or enhanced by e-beam irradiation, depending on the grating period. This effect is explained by competition of driving forces, which induce lateral mass transport accelerated by e-irradiation. The main driving forces are capillary (Laplace) force caused by variation of surface profile (it defines smoothing) and chemical force caused by deformed and broken chemical bonds under irradiation. We have calculated the kinetics of the profile

evolution assuming that the main mechanism of mass transfer is volume diffusion accelerated by irradiation. We have found that the flattening/enhancement constant depends on the grating wave number. Comparison the theory with the experiments shows that the calculated flattening/enhancement constant is in agreement with the experimental data. From the kinetics of both flattening and enhancement of SRGs, we have estimated effective diffusion coefficient inside the interaction volume: $D = 2.1 \times 10^{-10}\,\mathrm{m^2/s}$. The coefficient D is proportional to the concentration of radiation defects generated by e−irradiation. We conclude that similar effects of flattening/enhancement will occur under uniform illumination of similar surface gratings by band gap light that generates radiation defects in amorphous chalcogenides, in which irradiation-induced mass transport is observable.

ACKNOWLEDGMENTS

This work was supported by the TAMOP 4.2.2.A-11/1/KONV-2012-0036 project, which was co-financed by the European Union and European Social Fund.

[1]A. Zakery and S. R. Elliott, "Optical properties and applications of chalcogenide glasses: A review," J. Non-Cryst. Solids **330**(1-3), 1–12 (2003).
[2]J. Hu, Opt. Express **18**, 22174 (2010).
[3]N. Carlie, J. D. Musgraves, B. Zdyrko, I. Luzinov, J. Hu, V. Singh, A. Agarwal, L. C. Kimerling, A. Canciamilla, F. Morichetti, A. Melloni, and K. Richardson, Opt. Express **18**, 26728 (2010).
[4]H. Fritzsche, *Semiconducting and Insulating Glasses*, edited by P. Boolchand (World Scientific, River Edge, NJ, 2000), p. 653.
[5]A. V. Kolobov and S. R. Elliott, Adv. Phys. **40**, 625 (1991).
[6]S. R. Elliott, "Chalcogenide glasses," in *Materials Science and Technology*, edited by J. Zarzycki (VCH, Weinheim, 1991), Vol. 9.
[7]K. Tanaka and K. Shimakawa, *Amorphous Chalcogenide Semiconductors and Related Materials* (Springer, New York, 2011).
[8]A. Saliminia, T. V. Galstian, and A. Villeneuve, Phys. Rev. Lett. **85**, 4112 (2000).
[9]U. Gertners and J. Teteris, J. Optoelectron. Adv. Mater. **11**, 1963 (2009).
[10]M. L. Trunov, P. M. Lytvyn, P. M. Nagy, and O. M. Dyachyns'ka, Appl. Phys. Lett. **97**, 031905 (2010).
[11]M. L. Trunov, P. M. Lytvyn, and O. M. Dyachyns'ka, Appl. Phys. Lett. **96**, 111908 (2010).
[12]U. Gertners and J. Teteris, J. Optoelectron. Adv. Mater. **13**, 1462 (2011).
[13]Y. Kaganovskii, D. L. Beke, and S. Kökényesi, Appl. Phys. Lett. **97**, 061906 (2010).
[14]J. Teteris, U. Gertners, and M. Reinfelde, Phys. Status Solidi C **8**, 2780 (2011).
[15]Y. Kaganovskii, D. L. Beke, S. Charnovych, S. Kökényesi, and M. L. Trunov, J. Appl. Phys. **110**, 063502 (2011).
[16]K. Tanaka, Appl. Phys. Lett. **70**, 261 (1997).
[17]J. S. Romero, A. G. Fitzgerald, and K. Mietzsch, J. Appl. Phys. **91**, 9572 (2002).
[18]K. Shimikawa, N. Yoshida, A. Ganjoo, and Y. Kuzukawa, Philos. Mag. Lett. **77**, 153 (1998).
[19]K. Shimikawa and A. Ganjoo, J. Optoelectron. Adv. Mater. **3**, 167 (2001).
[20]G. B. Hoffman, W.-C. Liu, W. Zhou, R. Sooryakumar, P. Boolchand, and R. M. Reano, J. Vac. Sci. Technol. B **26**, 2478 (2008).
[21]C. Cserhati, S. Charnovych, P. M. Lytvyn, M. L. Trunov, D. L. Beke, Y. Kaganovskii, and S. Kokenyesi, Mater. Lett. **85**, 113 (2012).
[22]M. L. Trunov, P. M. Nagy, V. Takats, P. M. Lytvyn, S. Kokenyesi, and E. Kalman, J. Non-Cryst. Solids **355**, 1993 (2009).
[23]M. Trunov, P. Lytvyn, V. Takats, I. Charnovych, and S. Kokenyesi, J. Optoelectron. Adv. Mater. **11**, 1959 (2009).
[24]M. L. Trunov, C. Cserhati, P. M. Lytvyn, Y. Kaganovskii, and S. Kokenyesi, J. Phys. D: Appl. Phys. **46**, 245303 (2013).
[25]D. Drouin, A. R. Couture, D. Joly, X. Tastet, V. Aimez, and R. Gauvin, Scanning **29**, 92 (2007).
[26]D. B. Wittry and D. K. Kyser, J. Appl. Phys. **38**, 375 (1967).
[27]T. E. Everhart and P. H. Hoff, J. Appl. Phys. **42**, 5837 (1971).
[28]C. Thomas, I. Joachimsthaler, R. Heiderhoff, and L. J. Balk, J. Phys. D: Appl. Phys. **37**, 2785 (2004).
[29]W. van Roosbroeck, Phys. Rev. **91**, 282 (1953).
[30]H. Fritzsche, Semiconductors **32**, 850 (1998).
[31]Y. Kaganovskii, M. L. Trunov, D. L. Beke, and S. Kökényesi, Mater. Lett. **66**, 159 (2012).
[32]A. Regmi, A. Ganjoo, D. Zhao, H. Jain, and I. Biaggio, Appl. Phys. Lett. **101**, 061911 (2012).
[33]P. G. Shewmon, *Diffusion in Solids*, 2nd ed. (Wiley, New York, 1989).
[34]L. Reimer, *Scanning Electron Microscopy* (Springer-Verlag, Berlin, 1985).